Additive manufacturing of graded dielectrics

2014 Smart Mater. Struct. 23 045029

(http://iopscience.iop.org/0964-1726/23/4/045029)

IOP Publishing Smart Materials and Structures
Smart Mater. Struct. **23** (2014) 045029 (9pp) doi:10.1088/0964-1726/23/4/045029

Additive manufacturing of graded dielectrics

David A Roper[1], Brandon L Good[2], Raymond McCauley[3], Shridhar Yarlagadda[3], Jared Smith[1], Austin Good[1], Peter Pa[1] and Mark S Mirotznik[1]

[1] Department of Electrical and Computer Engineering, University of Delaware, Newark DE 19716, USA
[2] Naval Surface Warfare Center, Carderock Division, Bethesda, MD 20817, USA
[3] Center for Composite Materials, University of Delaware, Newark, DE 19716, USA

E-mail: droper@udel.edu and mmirotzni@udel.edu

Received 17 October 2013, revised 25 January 2014
Accepted for publication 28 January 2014
Published 6 March 2014

Abstract
A method for the fabrication of graded dielectrics within a structural composite is presented. This system employs an ultrasonic powder deposition head to print high dielectric powders onto a woven fabric composite substrate. It is shown how this system can integrate 3D variations of dielectric properties at millimeter resolution within a mechanically rugged substrate. To conclude, the system's practical application is demonstrated with experimental results from a graded index lens.

Keywords: graded dielectrics, dielectric properties, graded index lens, additive manufacturing, 3D printing

(Some figures may appear in colour only in the online journal)

1. Introduction

The ability to fabricate electromagnetic (EM) materials with graded dielectric properties would benefit a variety of interesting applications, such as low profile antennas [1, 2], antireflective surfaces [3], passive beam formers (e.g. Luneburg lenses) [4–7], graded index lenses [8, 9], and structural and armored radomes. A technique commonly used to synthesize graded dielectrics is subtractive manufacturing [3, 9]. There a computer numerically controlled (CNC) drill or milling machine produces a pattern of voids within a homogeneous dielectric material. Spatially varying the local volume fraction of the base dielectric grades the effective permittivity. While subtractive methods achieve reasonably good electromagnetic performance, the resulting part is often too fragile for many practical applications.

Recently there has been a surge in commercial 3D free-forming printing technologies. These systems employs additive manufacturing methods to create complicated 3D structures using a host of different techniques, including stereo lithography (SLA), fused deposition modeling (FDM) and selective laser sintering (SLS). While popular for a wide range of applications, commercial 3D printers use a limited library of materials that make them unsuitable for many EM applications including the fabrication of graded dielectrics. Thus, in this paper, a custom developed printer that is designed specifically for realizing materials with integrated three dimensionally varying dielectric properties is described. This system utilizes an ultrasonic dry powder deposition head, described in [10–15], to pattern high dielectric powders onto a low-loss dielectric substrate. After stacking and processing, the result is a mechanically rigid composite plate with an embedded 3D variation in dielectric properties. In section 2, a system level description of this printer including the materials, instrumentation and methodology used to locally tune dielectric properties is provided. In section 3, the calibration method and results are shown in detail. In section 4, an example of a graded index lens that is embedded within a structural composite is presented.

2. System design

The principal goal was to develop an additive manufacturing process capable of fabricating solid composite samples with

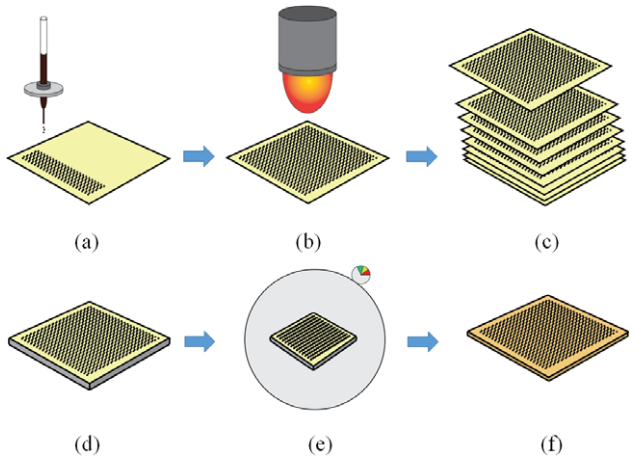

Figure 1. Overall flow diagram of 3D printing process. (a) Powder dispenses onto a composite substrate under computer control, (b) an IR spot heater adheres the powder to the substrate, (c) and (d) each printed layer is aligned and stacked, (e) an autoclave post-processes the stacked layers and (f) a solid composite with integrated dielectric properties results.

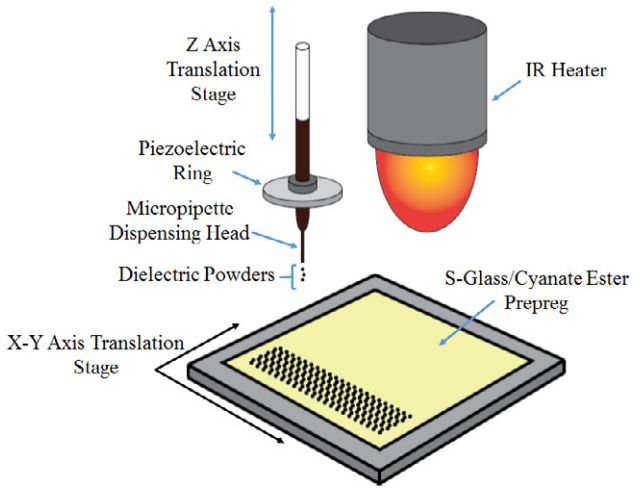

Figure 2. Illustration of the graded dielectric powder printer.

spatially varying dielectric properties. To this end, the custom printer, illustrated in figures 1 and 2, was designed, fabricated and tested.

Figure 1 presents a flow diagram illustrating the overall manufacturing process. The dielectric properties are controlled by dispensing high permittivity powders (HiK powder from Emerson and Cummings) onto a low-loss uncured composite substrate (S-glass/cyanate ester prepreg). The amount of powder dispensed in any small region determines the local effective permittivity. To produce a spatially varying permittivity, the print surface is moved under computer control and the amount of dispensed powder is varied (as shown in figures 1(a) and 2). After powder printing of each layer is completed, the pattern passes under an infrared spot heater for a brief period of time (<1 s/6 cm^2), long enough for the powder to adhere to the substrate but not enough for the cyanate ester resin to start curing (figure 1(b)). This step ensures that the powder pattern does not shift during later processing steps. Dielectric

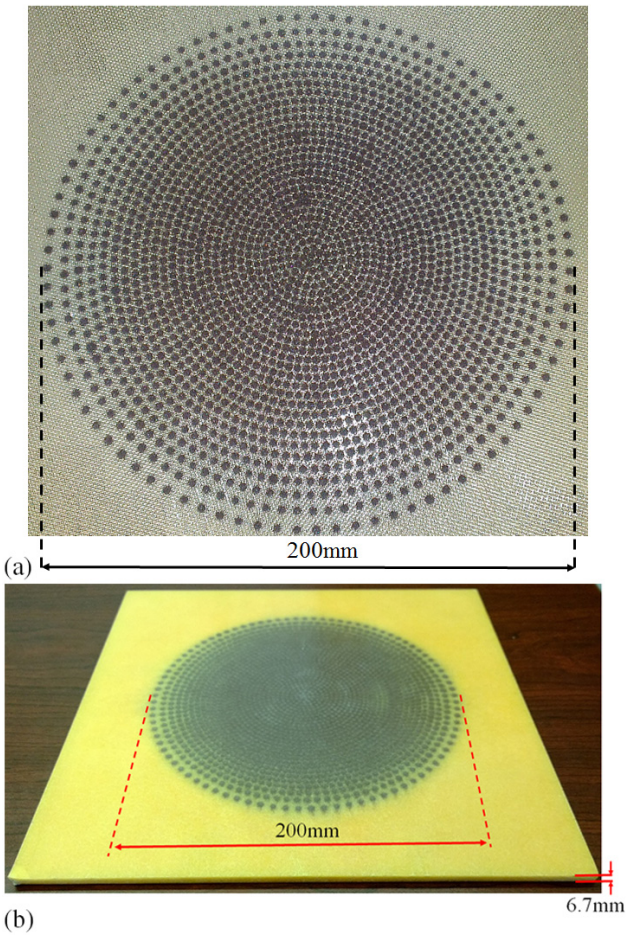

Figure 3. (a) Single layer of dielectric powder printed on a composite substrate before post-processing, and (b) final solid composite comprising an aligned stack of 16 printed layers shown in (a) after autoclave post-processing.

properties in the vertical or Z direction are varied by printing, aligning and stacking multiple layers (figures 1(c)–(d)). This multilayered stack is then transferred to an autoclave and subjected to high pressures (350 kPa) and high temperatures (450 K) for 1.5 h (figure 1(e)). The autoclave is needed to cure the resin within the composite substrate, to consolidate the layers and to remove any undesirable air bubbles. The final product is a dense composite sheet (similar to a Printed Circuit Board) with integrated powder that permanently maintains its proper spatial orientation (figure 1(f)). Figure 3(a) shows a panel that has been printed but not yet cured in the autoclave. Figure 3(b) shows the finished autoclaved 16 layer panel.

The following sections provide a more detailed description of the materials, instrumentation and calibration procedures.

2.1. Material selection

One of the most critical steps in this process is selecting the base materials, namely, the high dielectric constant powders and the base composite substrate. Both materials must not only satisfy electromagnetic constraints (i.e. low material loss and wide range of dielectric constants) but must also possess

attractive physical and mechanical properties. The materials selected were (1) S-glass/Cyanate Ester fiber reinforced composite prepreg (8 Harness Satin 6781, TenCate Inc.) as the base material and (2) ECCOSTOCK® HiK dielectric powder. The composite prepreg is a lightweight fabric (9 oz yd^{-2}) woven from S-glass fibers impregnated with a thermoset cyanate ester resin. This prepreg was chosen for its reasonably low dielectric constant ($\varepsilon_{glass} = 4.2$), low loss tangent (<0.01) and excellent structural properties. The same material is commonly used in high frequency circuit board applications and radomes. The HiK powder was chosen for its high dielectric constant ($\varepsilon_{HiK} = 12$) and low material loss at microwave frequencies This HiK powder also has a range of particle sizes (30–250 μm) that are well suited for the ultrasonic based deposition method described in the next section. Depending on the application other materials can be investigated without any major modifications to the manufacturing process. For example, adding ferrite powders to create graded magneto-dielectric composites is currently being explored.

2.2. Ultrasonic based dry powder deposition

To print a graded dielectric layer, a unique micro-dispensing dry powder applicator was constructed. This system integrates an ultrasonic based powder deposition system previously described by Yang *et al* [10–15]. The micro-dispenser is constructed using a glass micropipette and a piezoelectric ring ($D35 \times 15 \times 5$, Ultrasonic Supply) to effectively create an electronically controlled powder valve (see figure 4(a)). The pipette is tapered to match each powder's particle size so that it clogs under static conditions (see figure 4(b)). Yang *et al* showed that this clogging occurs when the diameter of the pipette tip, D, is no larger than approximately five times the diameter of the particles, d [12, 13].

When the piezoelectric ring that is rigidly mounted on the pipette is subjected to a short pulse of 42 kHz AC voltage, the dispensing head vibrates and ejects a small, yet repeatable amount of HiK powder [1]. This arrangement reliably dispenses HiK powder in quantities as small as 1.0 mg. An infrared spot heater (Model 4150, Research INC.) then adheres the powder to the substrate until it can be processed later in an autoclave.

2.3. Material post-processing

After printing and stacking, the part is placed in an autoclave for the final cure step. This step begins by placing the printed stack between a bottom release film and a top release film under a metal caul plate. The caul plate ensures that an even and consistent pressure is applied across the printed area (figures 5(a) and (b)). The part is then vacuum bagged before subjecting it to 350 kPa of pressure. Within the first hour, the autoclave temperature is increased by 2.5 K every minute until a maximum temperature of 450 K is reached. These conditions are held for an additional 1.5 h to ensure that the resin flows evenly throughout the part, encapsulates the added HiK powder, and fully cures. After a cool down period of about one hour, a fully cured, structural composite with the designed graded dielectric properties has been created (figure 5(d)).

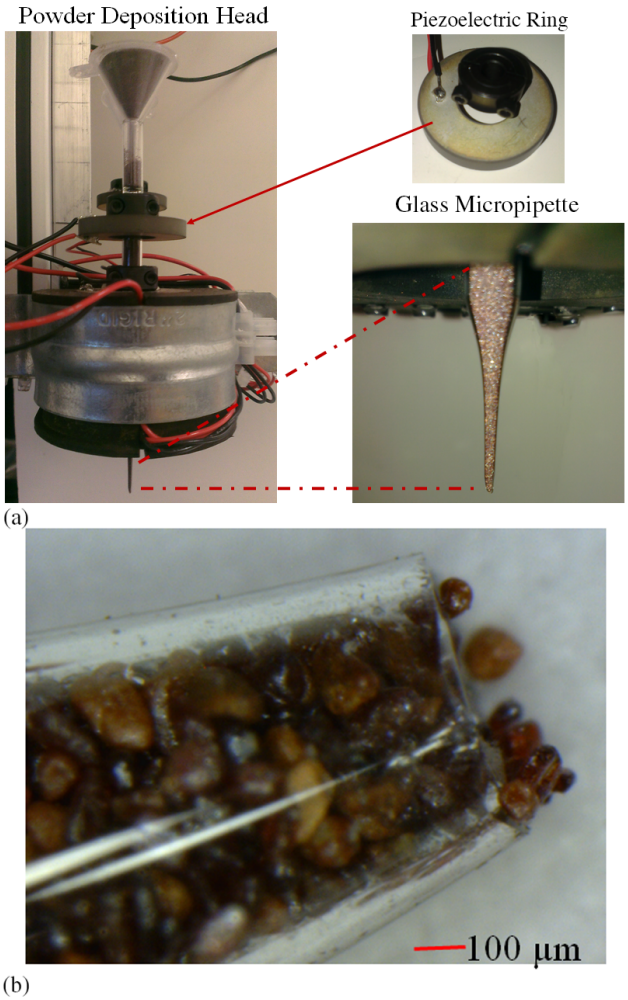

Figure 4. (a) Dry powder micro-dispenser. (b) 200× view of the tip of the micropipette filled with the high dielectric constant HiK powder.

2.4. Generating local dielectric properties through spatial dithering

As mentioned previously the effective dielectric constant is tuned at any X–Y plane position by locally varying the amount of HiK powder dispensed per unit surface area (mg mm^{-2}). To achieve this, a spatial dithering approach was implemented that is similar to the process used by commercial inkjet printers. With this approach small variable quantities (i.e. dots) of the high dielectric powder are dispensed onto the composite substrate following the pattern shown in figure 3. The amount of powder dispensed per unit area is spatially varied using one of two approaches. The first entails keeping the powder dot weight the same while varying the distance between dots (i.e. dot density) (figure 6(a)). This approach works well as long as the distance between dots is small compared to the operational electromagnetic wavelengths. If this is not the case, undesirable diffractive effects will occur. The second approach involves varying the powder dot weight while maintaining a fixed distance between dots (figure 6(b)). A variable dot weight is achieved by exciting the dispenser with a control signal of variable pulse widths. It was found that this approach was most useful when dense patterns were

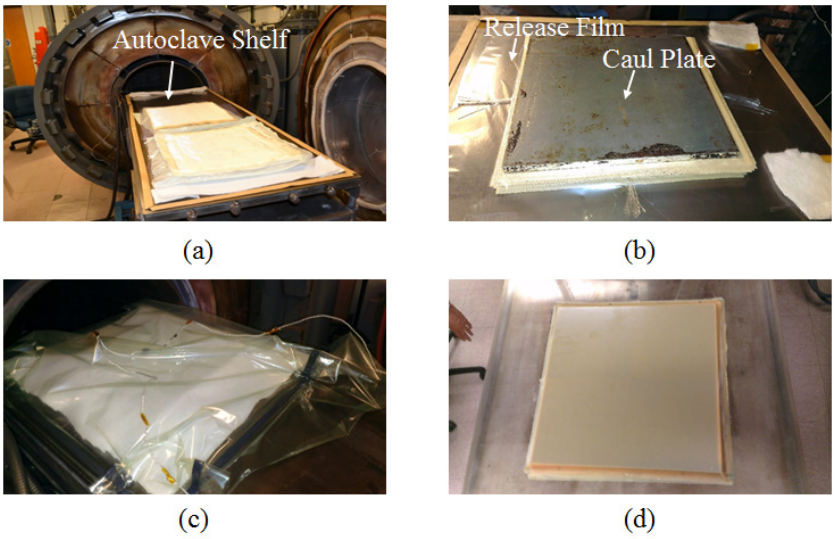

Figure 5. Post-processing of material in autoclave. (a) Composite sample is placed on a release film on the autoclave shelf, (b) a caul plate is added, (c) the sample is vacuum bagged, heated and compressed, and (d) the final composite is created.

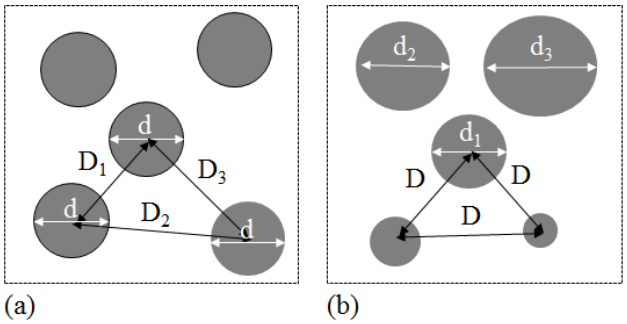

Figure 6. Illustration of the two spatial dithering methods used to generate effective dielectric properties. (a) Fixed powder weight with variable spacing, and (b) fixed spacing with variable powder weight.

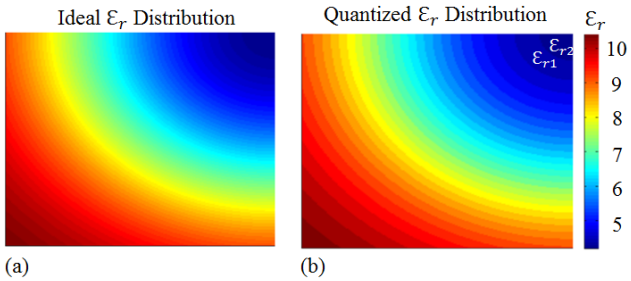

Figure 7. (a) Desired continuous graded dielectric distribution. (b) Distribution in 7(a) quantized into a finite number of homogeneous regions.

needed that still achieved the expected dielectric constant. Both approaches shown in figure 6 provide similar dielectric constants as long as (1) the distance between dots is much smaller than the electromagnetic wavelengths, and (2) the volume or weight fraction of powder per unit area is the same. The experimental calibration method described in section 3 was used to determine the relationship between the powder weight per unit area and the effective dielectric constant.

2.5. Algorithms for spatially varying dielectric properties in a 2D plane

In this section the algorithms are presented for mapping a desired two-dimensional dielectric distribution into a powder dot pattern that the printer can realize. As an example, an arbitrary two-dimensional dielectric distribution, illustrated in figure 7(a), was chosen. The algorithms begin by quantizing the continuous dielectric distribution into a number of homogeneous regions (figure 7(b)). Then they proceed for the constant and variable dot weight approaches (figures 6(a) and (b), respectively) as described below.

2.5.1. Fixed dot weight. This method achieves the proper effective dielectric properties by placing powder drops of a fixed weight and varying the distance between these dots. For each region, the amount of powder per unit area is determined from a look-up table. This look-up table has been pre-calculated employing the calibration method described in section 3. A commercial finite-element meshing program then divides each of the homogeneous regions (illustrated in figure 7(b)) into a mesh of triangular elements of nearly equal area (figure 8(a)). The centroid of each of these triangular elements gives the xy coordinates of the powder dots (figure 8(b)). This algorithm effectively produces a partitioned region for each drop of dielectric powder that maintains the proper powder weight to area ratio needed to achieve the desired effective dielectric constant. This process, although complicated, was found to be quite robust.

2.5.2. Variable dot weight. This alternative algorithm divides the entire region of interest into a grid of equal sized cells (figure 9). At the center of each cell, dielectric powder is dispensed with a variable dot size. The size of the unit cell is set by the largest amount of powder that can be dispensed yet still can adhere to the substrate. For this system, it was

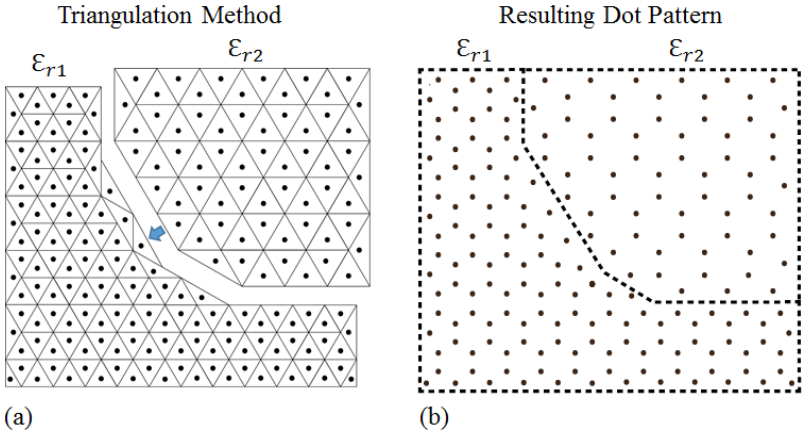

Figure 8. (a) Each homogeneous region is divided into triangular elements of approximately equal area using a commercial finite-element meshing program. Dots indicate each element's centroid. (b) The centroids determine the locations of the powder dots.

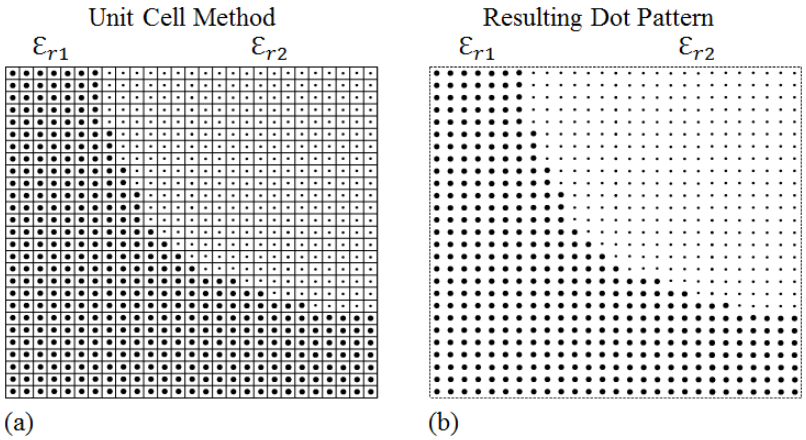

Figure 9. (a) Desired surface is divided into rectangular elements of equal area. (b) The amount of powder in each of these elements is calculated to determine the desired effective dielectric constant.

determined that a powder dot size of approximately 3 mm in diameter was the largest that the printer could reliably dispense and get to adhere to the substrate. This gave a unit cell size of ~9 mm^2. Once a unit cell size had been determined, the designed dielectric constant to these unit cells could be mapped using the same look-up table used for the fixed dot algorithm.

2.6. Dielectric variations in the third dimension

To generate a spatial variation in permittivity in the z-direction, multiple xy layers are simply printed, aligned and stacked before processing. Admittedly this is a more manual process than most 3D printers. The resolution in this 3rd dimension is set by the thickness of each printed layer. With the materials outlined in section 2.1, the typical thickness of a single printed layer is 0.25–0.4 mm depending on the amount of added powder.

3. Calibration

To determine the relationship between the local powder density (mg mm^{-2}) and the effective dielectric constant, a set of calibration measurements were conducted. Using the fixed dot size manufacturing process described above, seven different samples of different powder weight densities were fabricated and experimentally characterized. Each sample comprised eight identically printed layers that were aligned, stacked and post-processed as described previously. Figure 10 shows the top layer of a typical calibration sample before post-processing. After each sample was post-processed, their dielectric properties were measured between 4.0 and 30 GHz using a free-space focused beam measurement system at the Naval Surface Warfare Center, Carderock Division (figure 11).

Results from the calibration experiments are summarized in table 1 and figure 12. For the calibration samples, the powder weight density (w) was varied from 0 mg mm^{-2} (sample #1) to 0.51 mg mm^{-2} (sample #7). The 0.51 mg mm^{-2} value was near the maximum amount of dielectric powder that could be dispensed and could still adhere to the substrate. Over this range of densities, the effective dielectric constant varied from 4.2 to 10.7. Notably, the loss tangent was quite small over the entire frequency range ($<$0.005). In addition, the effective dielectric properties were free from any undesirable diffractive effects as long as the periodicity of the powder pattern, denoted

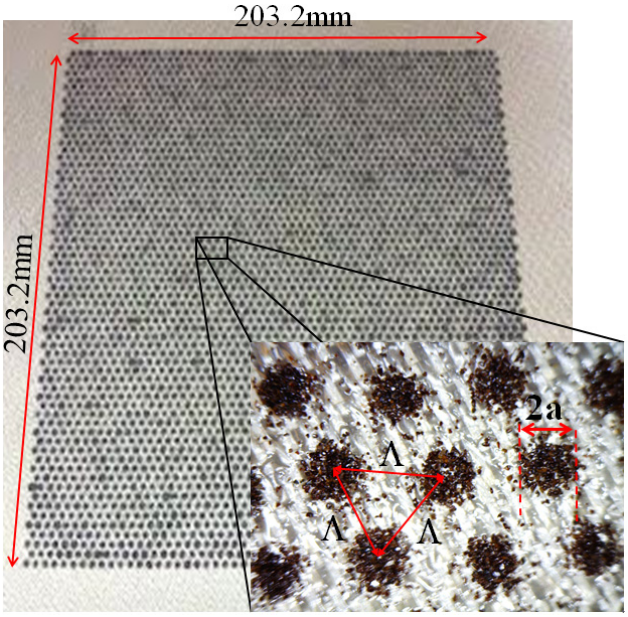

Figure 10. Photograph of a sample that was created using a fixed powder weight, spatial dithering approach to achieve a homogeneous dielectric constant over the pattern. Inset gives higher magnification showing the dots of diameter $2a$ with spacing of Λ.

Table 1. Dielectric and weight properties of graded dielectric panels.

Sample no.	w (mg mm^{-2})	ε_r
1	0	4.2
2	0.14	5.3
3	0.20	6.2
4	0.32	7.4
5	0.41	8.9
6	0.44	9.3
7	0.51	10.7

Λ in figure 10, was less than 5.0 mm. Moreover, over the entire 4–40 GHz band there was no significant frequency dependence.

The measured effective permittivity, ε_{eff}, was found to satisfy the modified Maxwell–Garnet distribution given by

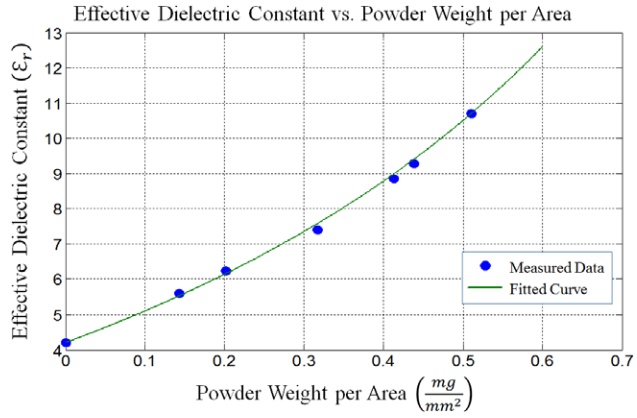

Figure 12. Measured dielectric constant versus powder weight per square millimeter. Measurements were conducted between 4 and 30 GHz using a free-space focused beam measurement system. Also shown is a modified Maxwell–Garnet distribution equation (1) used to fit the experimental data.

$$\varepsilon_{\text{eff}} = \varepsilon_{\text{m}} \frac{\varepsilon_i(1+2(\alpha * w)) - \varepsilon_{\text{m}}(2(\alpha * w) - 2)}{\varepsilon_{\text{m}}(2+(\alpha * w)) + \varepsilon_i(1-(\alpha * w))} \tag{1}$$

where ε_{m} and ε_i denote the dielectric constant of the substrate and the HiK dielectric powder, respectively, w is the powder weight density (mg mm^{-2}) and α denotes a calibration factor. A value for α of 1.45 (mm^2 mg^{-1}) was determined empirically and provided a good fit of the experimental results.

With these calibration results, a graded dielectric profile could be mapped to a powder weight density distribution that could be realized. The next section provides an illustrative example of this process.

4. Example: graded index lens

To demonstrate the capabilities of this new printer, a graded index (GRIN) lens (figure 13) was designed, fabricated and experimentally characterized. This lens is a flat GRIN lens designed to focus an incoming plane wave of 30 GHz center frequency onto a focal plane at a distance of 500 mm.

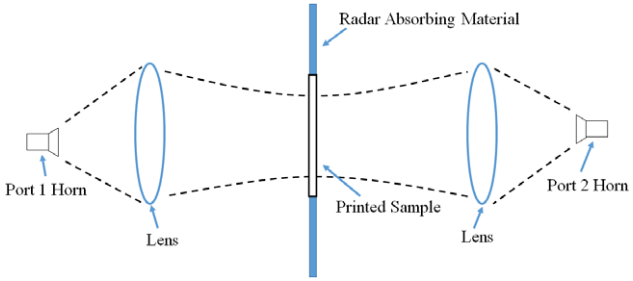

Figure 11. Free-space focused beam measurement system.

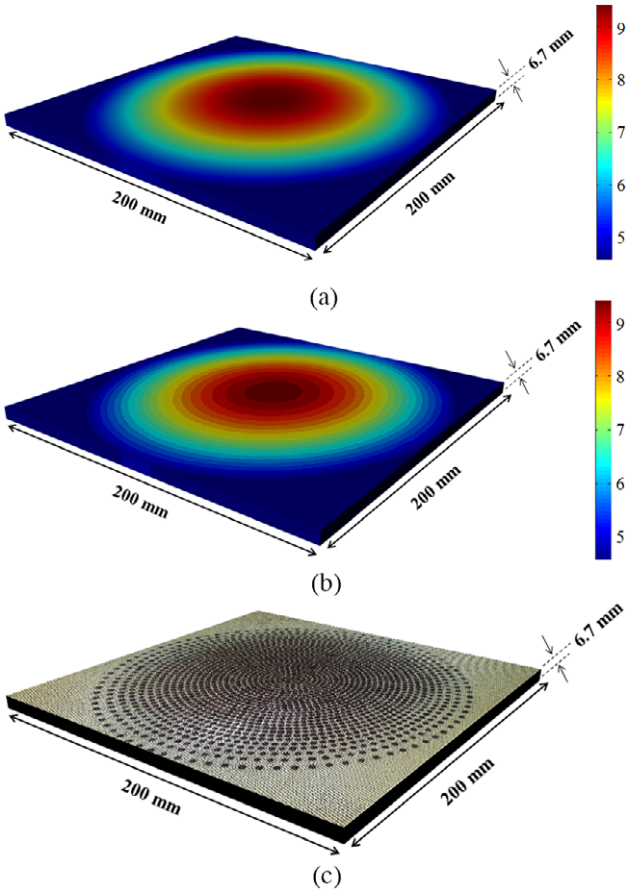

Figure 13. Graded index lens design. The lens was designed to focus a 30 GHz plane wave at a distance of 500 mm from the surface of the lens. (a) Desired continuous graded dielectric profile. (b) Desired quantized graded dielectric profile. (c) Computed powder dot pattern.

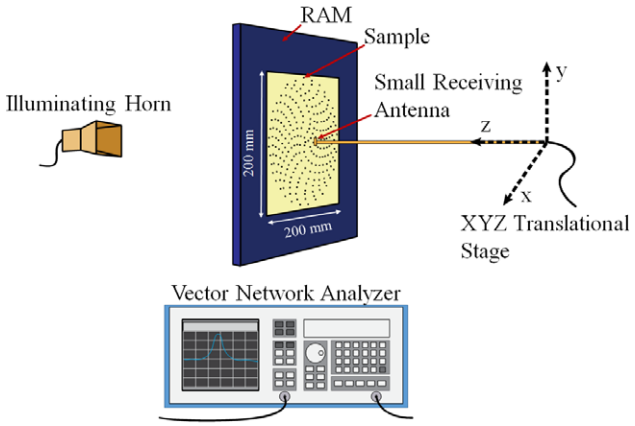

Figure 14. Illustration of test setup used to experimentally characterize the fabricated samples.

4.1. Design algorithm for GRIN lens

To generate the proper phase distribution at its output aperture, a GRIN lens follows a graded dielectric distribution given by:

$$\varepsilon_{\text{eff}}(r) = \left(\sqrt{\varepsilon}_{\text{m}} - \frac{\sqrt{f^2 + r^2} - f}{d}\right)^2 \qquad (2)$$

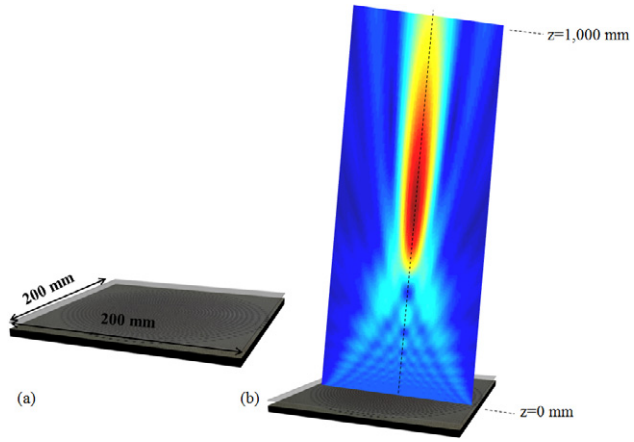

Figure 15. Illustration of experimental scans used to measure the response of the graded index lens sample. (a) 2D scan in a plane across the surface of the lens. The detector was placed a very short distance (∼2 mm) from the surface of the sample. (b) Line scan through the optical axis (dashed line).

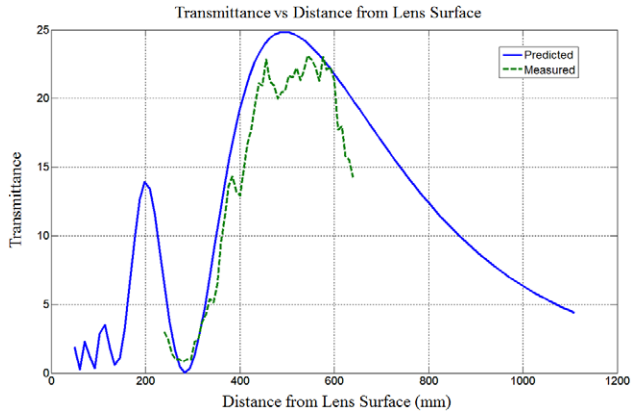

Figure 16. Measured and predicted transmittance along the optical axis shown in figure 15(b).

where r is the radial distance from the center of the lens, f is the focal length, ε_{m} is the maximum permittivity at the center of the lens, and d is the lens thickness. For this example, a lens aperture of 200 mm × 200 mm and a thickness of $d = 6.7$ mm was assumed. The maximum permittivity, which was provided by equation (2), to be $\varepsilon_{\text{m}} = 9.5$, and the minimum permittivity was taken as that of the substrate, $\varepsilon_{\text{s}} = 4.5$. Figure 13(a) depicts the desired permittivity distribution.

To map this permittivity distribution given by equation (2) to a geometrical pattern that can be printed, the fixed dot size algorithm described in section 2.5.1 was used. This process quantized the desired continuous distribution into discrete permittivity values (figure 13(b)). Within each region, the algorithm selected the powder dot density that best matched the desired local refractive index using the pre-calculated calibration curve described in the previous section. The final dot pattern is illustrated in figure 13(c).

4.2. Fabrication and experimental characterization

The graded index lens shown in figure 13 was fabricated using the powder printer previously described. After post-

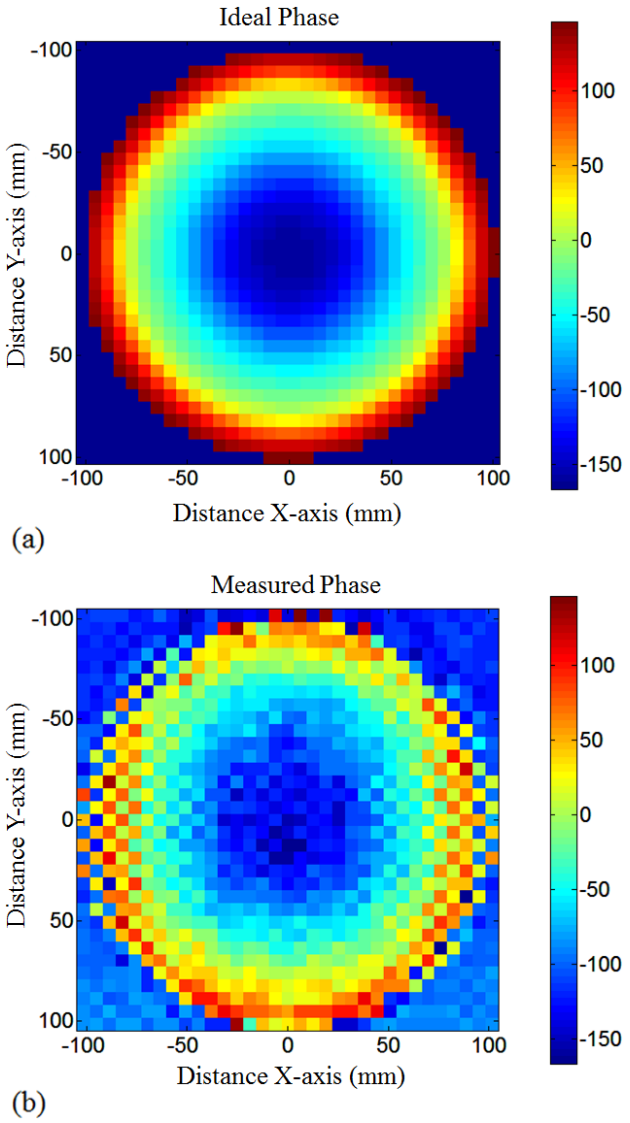

Figure 17. Desired (a) and measured (b) phase distribution in degrees across the surface of the lens shown in figure 15(a). The data were collected at an incident frequency of 30 GHz.

processing, the result was a flat, solid composite plate shown in figure 3(b).

To characterize this fabricated sample, the setup depicted in figure 14 was used. At the heart of this setup is an Agilent PNA Vector Network Analyzer (VNA) with external heads that extend the frequency range from 20 MHz to 110 GHz. On the transmitting side, a standard gain horn, placed in the far-field of the sample, creates a quasi-plane wave at the surface of a square entrance aperture that is 200 mm $\times$ 200 mm in size. The sample is surrounded with radar absorbing material (RAM) to minimize diffraction effects from the edges. On the receiving side, a small receiving antenna attached to a xyz translation system measures the transmitted magnitude and phase as a function of space. An external computer controls and coordinates xyz translation and VNA measurements. The entire setup was constructed inside a larger chamber covered with radar absorbing material on all surfaces to minimize external interference. Extraneous reflections were also removed using frequency averaging and time-domain gating.

4.3. Results

The experimental characterization results are provided in figures 16 and 17. Figure 16 plots the normalized intensity (i.e. transmittance) of the lens measured along the optical axis depicted by the dashed line in figure 15(b). These measured results are compared to simulations that were computed using the commercial finite-element program HFSS. The measured transmittance closely matches the simulated curve, both indicating that focus occurs approximately 500 mm from the surface of the lens.

Figure 17 shows the measured and desired 2D phase response near the surface of the lens. For these plots, a normally incident plane wave at 30 GHz was assumed. The measured results (figure 17(b)) have the same phase characteristics as the desired phase distribution (figure 17(a)). Thus the sample was able to effectively mirror the graded dielectric properties that were desired.

5. Conclusion

In this paper an additive manufacturing method was described that realizes graded dielectrics within a structural composite. This method employs an ultrasonic powder dispenser to permanently embed a 3D spatially varying permittivity within a solid fiberglass composite panel. An application of this new printer was demonstrated by designing, fabricating and experimentally characterizing a graded index lens. Future work will focus on extending this method to additional materials (e.g. magnetic powders) and applications.

References

[1] Sabet K, Ozdemir T, Frantzis P, Sarabandi K and Katchi L P B 2002 Compact wireless antennas using an artificial dielectric lens *2002 IEEE Aerospace Conf. Montana, USA* vol 2, pp 931–937

[2] Bukhari H and Sarabandi K 2013 Ultra-wideband printed slot antenna with graded index superstrate *IEEE Trans. Antennas Propag.* **61** 5278–82

[3] Mirotznik M, Good B, Ransom P, Wikner D and Mait J 2010 Broadband antireflective properties of inverse motheye surfaces *IEEE Trans. Antennas Propag.* **58** 2969–780

[4] Sato K and Ujiie H 2002 A plate Luneberg lens with the permittivity distribution controlled by hole density *Electron. Commun. Jpn.* **85** 912–22

[5] Xue L and Fusco V F 2007 Patch fed 2D planar Luneburg lens *Microw. Opt. Technol. Lett.* **49** 2922–4

[6] Xue L and Fusco V F 2008 Printed holey plate Luneburg lens *Microw. Opt. Technol. Lett.* **50** 378–80

[7] Rondineau S, Himdi M and Sorieux J 2003 A sliced spherical Luneburg lens *IEEE Antennas Wirel. Propag. Lett.* **2** 163–6

[8] Good B, Ransom P, Simmons S, Good A and Mirotznik M S 2012 Design of graded index flat lenses with integrated antireflective properties *Microw. Millimeter Wave Technol. Lett.* **54** 2774–81

[9] Wu Q, Turpin J, Wang X, Werner D, Pogrebnyakov A, Swisher A and Mayer T 2012 Flat transformation optics graded index lenses *European Conf. Antennas and Propagation* pp 1701–1705
[10] Lu X, Yang S and Evans J 2009 Microfeeding with different ultrasonic nozzle designs *Ultrasonics* **49** 514–21
[11] Yang S and Evans J 2007 Metering and dispensing of powder: the quest for new solid free forming techniques *Powder Tech.* **178** 56–72
[12] Lu X, Yang S and Evans J 2007 Dose uniformity of fine powders in ultrasonic microfeeding *Powder Tech.* **175** 63–72
[13] Yang S and Evans J 2004 Acoustic control of powder dispensing in open tubes *Powder Tech.* **139** 55–60
[14] Lu X, Yang S and Evans J 2008 Ultrasound-assisted microfeeding of fine powders *Particuology* **6** 2–8
[15] Yang S and Evans J 2004 A dry powder jet printer for dispensing and combinatorial research *Powder Tech.* **142** 219–22